Aggregation of a quenched Lennard-Jones system under shear

B. D. Butler and H. J. M. Hanley
Thermophysics Division, National Institute of Standards and Technology, Boulder, Colorado 80303

D. Hansen and D. J. Evans
Research School of Chemistry, Australian National University, Canberra, ACT 0200, Australia
(Received 5 July 1995)

The thermodynamic decomposition of an unstable thermostatted system of Lennard-Jones disks is investigated by nonequilibrium molecular dynamics. The system, first unsheared and then subjected to planar Couette flow, is studied after temperature quenches into the unstable vapor-liquid and the vapor-solid coexistence regions of the phase diagram. An interconnected morphology, characteristic of spinodal decomposition, forms after quenching. The cluster growth is found to be temporally self-similar, and the structure factor $S(q,t)$ obeys the dynamic scaling relation $S(q,t) \sim q_m^{-d_f}(t)\tilde{S}[q/q_m(t)]$. Here, q is the scattered wave vector magnitude, $q_m(t)$ is the location of the low angle peak in $S(q,t)$, $\tilde{S}(x)$ is a time-independent structure function which has a maximum at $x=1$, and d_f is a fractal dimension. d_f is relatively insensitive to the postquench state point, but may depend on the shear rate. The primary influence of shear is to accelerate the aggregation—an effect that has also been observed experimentally in dense gelling silica suspensions. The similarities between these simulations and experiment suggest that a characteristic fractal dimension of a dense gel may be determined from measurements of $S(q,t)$.

I. INTRODUCTION

This paper describes the simulated thermodynamic decomposition of two-dimensional Lennard-Jones systems after quenching into unstable regions of the phase diagram. Specifically, we quenched from the fluid at three different densities to (a) a temperature between the critical and triple points, and (b) to a temperature below the triple point. Spinodal decomposition from within the vapor-liquid coexistence region has been investigated in some detail previously,[1] but this is an attempt to study decomposition of a single-component system quenched from above the critical temperature to the unstable vapor-solid coexistence region. Furthermore, the simulations were based on the technique of nonequilibrium molecular dynamics[2] (NEMD) so we were able to explore the effect of shear on the decomposition processes.

The work was stimulated in part as a way to explain recent results from small-angle neutron-scattering (SANS) experiments on the gelling of dense colloidal silica suspensions.[3] It is now common to interpret the crystal growth of colloidal systems in terms of the nucleation and growth or spinodal decomposition theories developed for simple liquids and alloys.[4,5] An obvious extension is to apply these concepts to gel formation. Specifically, we equate the aggregation that occurs during gel formation with a spinodal decomposition mechanism following a quench.

The simulations follow naturally from our previous investigations on simple sheared liquids.[6] In earlier studies, we have used NEMD to stimulate simple liquids subjected to an applied shear γ and have demonstrated that γ can be considered as a thermodynamic state variable.[6,7] Because a sheared system has phase behavior which is perturbed, or even qualitatively different, from that described by the equilibrium phase diagram, we anticipated that shear would influence the decomposition process after a quench and, by extension, the aggregation process which results in gel formation.[8,9] We show that shear does, in fact, effect the decomposition of a quenched Lennard-Jones system, and the paper includes a discussion of these effects.

Figure 1 outlines the equilibrium phase diagram of the 2D single-component Lennard-Jones system. Solid lines in the figure indicate the coexistence boundaries. The vapor-liquid and liquid-solid boundaries were obtained from liquid-state perturbation theory and Monte Carlo simulations.[10] The vapor-solid coexistence boundaries are extrapolations from the triple-point line to zero temperature using the reduced densities of 0 for the vapor and $^3\sqrt{4}/\sqrt{3} \approx 0.92$ for the solid. It is appreciated that the exact placement of the lines—particularly the location of the critical and triple points—depend on details of the simulation, such as system size and potential cutoff.[11] These details, however, are not important

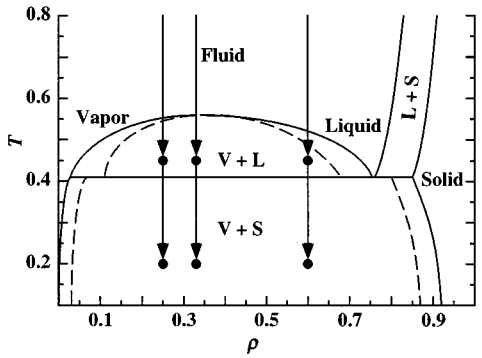

FIG. 1. Phase diagram for the 2D Lennard-Jones system. Simulated quenches were to the six state points indicated by ●. The dashed lines indicate spinodal boundaries—those inside the vapor-solid coexistence region are speculative.

for our purposes. The dotted lines mark the spinodes—the limits of mechanical stability. The vapor-liquid spinodal boundary, obtained from liquid-state perturbation theory, is taken from Henderson.[12] The vapor-solid spinodes are intended to be only schematic since their location in the vapor-solid coexistence region is unknown. The vertical lines in Fig. 1 symbolize our simulation paths: the system is equilibrated as a fluid above the critical temperature and then quenched to state points below the critical and/or triple points into the mechanically and thermodynamically unstable regions of the phase diagram.

Central to our theme is the behavior of the structure factor $S(q,t)$ as a function of time t and wave vector q. Theoretical treatments of spinodal decomposition in general, and predictions for the time evolution of $S(q,t)$ in particular, have been presented for binary solutions by Cahn and others,[13–15] and for the one-component fluid in equilibrium with its vapor by Abraham.[16] In the theory of Cahn-Hilliard-Cook[13,14] the earliest stages of decomposition are characterized by the growth in amplitude of compositional fluctuations of a particular wave vector magnitude. At early times, therefore, a peak will appear in $S(q,t)$ at this characteristic wave vector. This peak then grows in amplitude without significant shift in wave vector. At later times, when the fluctuation amplitudes have reached approximately the densities dictated by the equilibrium phase boundaries, the structure will coarsen by interfacial dynamics. In this late coarsening regime, the peak in $S(q,t)$ continues to grow in height but now moves towards lower q, reflecting the increasing average domain size of the two phases. Decomposition after a quench to inside the spinodal can thus be characterized by three time regimes: an early stage described by the linear Cahn-Hilliard-Cook theory, a late time coarsening regime, and a crossover regime separating these two limits.[17] Cahn[14] has shown that the microstructures in the early time (linear) regime are highly interconnected—a feature often viewed as characteristic of spinodal decomposition.

The time over which the early stage decomposition proceeds is dictated by both the $t=0$ correlation length and the particular location inside the unstable region to which the system has been quenched.[17–19] When the particle-particle correlation distance is small or the quench is far inside the unstable region, the early time regime may be very short lived or even nonexistent. The correlation distance in our initial high-temperature configuration is short range and the quenches simulated here are all deep within the unstable region (Fig. 1). Hence, we expect to see a peak in $S(q,t)$ which both grows and shifts toward lower q as the system evolves, that is, behavior characteristic of the late stage coarsening regime of a system quenched below the spinodal.

A gelling colloidal suspension is characterized by short-range interactions.[20] Hence these simulations are particularly relevant as tools to interpret gelation experiments. Real-space particle imaging is possible, in principle, but extremely difficult to carry out in practice. In the simulation, however, we can quench a system and follow the decomposition by monitoring both $S(q,t)$ *and* the real-space particle cluster morphology. We can thus study the evolution of $S(q,t)$ in detail and connect the variation of $S(q,t)$ to known cluster formations. The qualitative behavior of our two-dimensional simulations will certainly allow us to understand better the experimental data.

The paper is organized as follows. Section II outlines the procedure and computer technique which we use to investigate the quenches and subsequent evolution of the postquenched system, both with and without an applied shear. Section III reviews the results and compares the behavior of the structure factor with plots of the cluster morphologies. The evolution of $S(q,t)$, is discussed in Sec. IV. The connection between the simulation data and experiments with real silica gels are briefly summarized in Sec. V. Conclusions end the paper.

II. PROCEDURE

We consider a thermostatted two-dimensional system of N Lennard-Jones (LJ) particles subjected to planar Couette flow. The particles have unit mass and interact with the dimensionless potential,

$$\phi_{\mathrm{LJ}}=4\left[\left(\frac{1}{r}\right)^{12}-\left(\frac{1}{r}\right)^{6}\right], \tag{1}$$

where $r=|\mathbf{r}_i-\mathbf{r}_j|$, with $\mathbf{r}_i$ the position of particle i $(i=1,N)$. The density of the system is defined as $\rho=N/A$, where A is the area; the temperature is taken as the kinetic temperature T. The shear rate is defined by $\gamma=\partial u_x/\partial y$, with u_x the x component of the streaming velocity $\mathbf{u}$. Calculations were carried out with $N=14\,336$ with the LJ potential cutoff at 2.5. A few runs were made with $N=3584$ in order to investigate the influence of system size.

Initial values of the particle positions and peculiar momenta $\mathbf{p}_i$ were assigned at $T=1$ and the system equilibrated. The system's behavior was studied after temperature quenches into the vapor-liquid and vapor-solid coexistence regions. Figure 1 traces the path of six quenches simulated at $\rho=0.25$, 0.325, and 0.6 to a temperature $T=0.45$ and to a temperature $T=0.2$. The quenched system was then allowed to evolve without the presence of an applied shear and then when subjected to shears of $\gamma=0.01$ and 0.1 at $T=0.45$, and $\gamma=0.01$ at $T=0.2$.

The simulations were based on the nonequilibrium molecular dynamic (NEMD) shear algorithms discussed extensively by Evans and co-workers.[2] All computations were performed using a 128-processor parallel supercomputer. Details of the computational procedure and the parallelization scheme for planar Couette flow can be found in Ref. 21. In outline, however, the NEMD technique solves the thermostatted equations of motion[2] set up to mimic Couette flow for the system with Lees-Edwards periodic boundary conditions at a given shear rate and temperature:

$$\frac{d\mathbf{r}_i}{dt}=\frac{\mathbf{p}_i}{m}+\mathbf{n}_x\gamma y_i\,, \tag{2}$$

$$\frac{d\mathbf{p}_i}{dt}=\mathbf{F}_i-\mathbf{n}_x\gamma p_{iy}-\alpha\mathbf{p}_i\,, \tag{3}$$

where $\mathbf{n}_x$ is a unit vector in the flow direction and the force, $\mathbf{F}_i=-\Sigma_j\partial\phi_{LJ}(r)/\partial\mathbf{r}_i$. The equations include the thermostatting multiplier α given by

$$\alpha = \sum_{i-1}^{N} \mathbf{p}_i \cdot \mathbf{F}_i \Big/ \sum_{i-1}^{N} \mathbf{p}_i \cdot \mathbf{p}_i . \tag{4}$$

For all runs, the system was first equilibrated in the fluid at $T=1$, and then quenched into the unstable region to a state point indicated in Fig. 1. The time step was set at $\Delta t = 0.004$ and the simulation monitored over at least 250 000 time steps (i.e., until $t=1000$). The shear simulations were run at low Reynolds numbers, hence the peculiar velocity of any particle, i, is given unambiguously by $\mathbf{p}_i/m$ in Eq. (2) and the kinetic temperature is defined in the usual way by $T=\Sigma_i(\mathbf{p}_i^2)/2mNk_B$, where k_B is Boltzmann's constant. Because in each of these simulations $\gamma \ll 1$, the results will be independent of the thermostat employed (i.e., the heating rates are small). Key data are plots of the positions of the particles as a function of time for a given state point—that is, the morphology of the system—and the corresponding structure factor.

The azimuthally averaged structure factor was evaluated for a particular simulation by first counting the number of particle pairs N_r separated by distances between r and $r+\Delta r$ in the range $r=0 \rightarrow a/\sqrt{2}$, where a is the edge length of the simulation box, with $\Delta r = 0.01$. In the range $r=a/2 \rightarrow a/\sqrt{2}$ care was taken to count only those pairs separated by the shortest distance after taking account of the periodic boundaries. N_r thus decreases rapidly from its maximum at $r=a/2$ to zero at $r=a/\sqrt{2}$. The structure factor was computed from this distribution using

$$S(q) = \frac{1}{N} \sum_{r=0}^{a/\sqrt{2}} (N_r - N_r^{\mathbf{av}}) J_o(2\pi q r), \tag{5}$$

where J_o is the spherical Bessel function of order 0 (which takes account of the azimuthal averaging) and N_r^{av} is the number of particle pairs expected from a random (uniform density) placement of particles. $S(q)$ was first computed in increments $\Delta q/2\pi = 0.0025$ and then smoothed using a running average with a window size $\Delta q/2\pi = 0.01$.

With finite-size simulations, the subtraction of N_r^{av} in Eq. (5) plays an important role as it efficiently subtracts the ''average'' scattering associated with the simulation box shape and size. Scattering from the simulation box, if not subtracted, will result in a sharp spike at the reciprocal space origin (of width related to the reciprocal of the simulation box size), and will also produce several unwanted decaying ''interference fringes'' at higher q.[22] Careful counting of the particle pairs at distances between $r=a/2 \rightarrow a/\sqrt{2}$ causes the Bessel summation to be smoothly truncated. If this were not done, $S(q)$ may have the artificial oscillations often encountered when computing $S(q)$ from normalized pair distributions. The running average also helps to minimize the unavoidable oscillations resulting from the finite system size.

III. RESULTS

Our basic results are summarized by the sequence of events shown in Fig. 2. This figure displays the time evolution of the system after a quench to $T=0.2$ at a density $\rho=0.325$ for shears of $\gamma=0$ and 0.01. We see that the particles of the system at $\gamma=0$—which showed initially the characteristic distribution of a fluid at $T=1$—have already aggregated at $t=8$, and that these aggregates form a fine-scale interconnected morphology. As the system evolves it coarsens. A striking feature of this coarsening process is that, except for a change in length scale, the system at the early time looks just like the system at the later times. In other words, the system displays temporal self-similarity. The effect of the shear is also pronounced; the coarsening process appears to proceed in a comparable fashion when the shear is applied, only shear has substantially accelerated the aggregation until the simulation box is filled effectively by one cluster at $t=1000$.

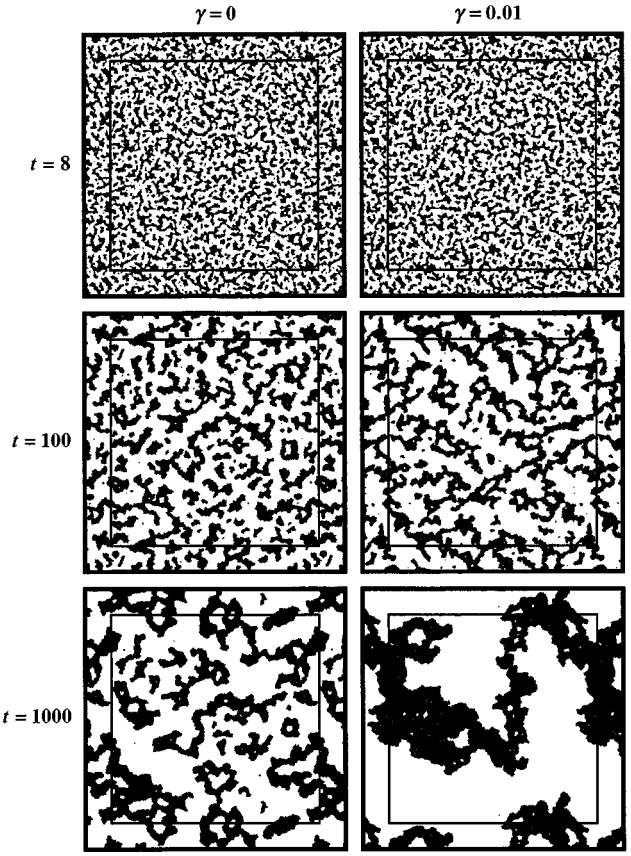

FIG. 2. Decomposition of a Lennard-Jones system of density $\rho=0.325$, quenched to a temperature $T=0.2$. γ is the shear rate and t is the time since the system was quenched. The simulations contain $N=14\,336$ particles and the inner rectangles indicate the simulation box size.

Figure 3 displays the computed structure factors corresponding to the images of Fig. 2 and the time dependence of the location of the maximum value of $S(q,t)$. Shown are $S(q,t)$ plotted against the parameter $q/2\pi$. We first note that $S(q,t)$ for $q/2\pi > 1$ indicates a close-packed internal distribution of a solid, even at the earliest displayed time of $t=8$. These peaks sharpen with time because the size of the clusters increase (not, as might be assumed, because the solid becomes more ordered). This is made clear from the magnified, but representative, real-space images of Figs. 4(a) and 4(b) which are taken from the simulations shown in Fig. 2.

The curves of Figs. 3(a) and 3(b) display an apparent power-law increase in the structure factor with decreasing q. This power-law behavior, however, is simply an artifact that

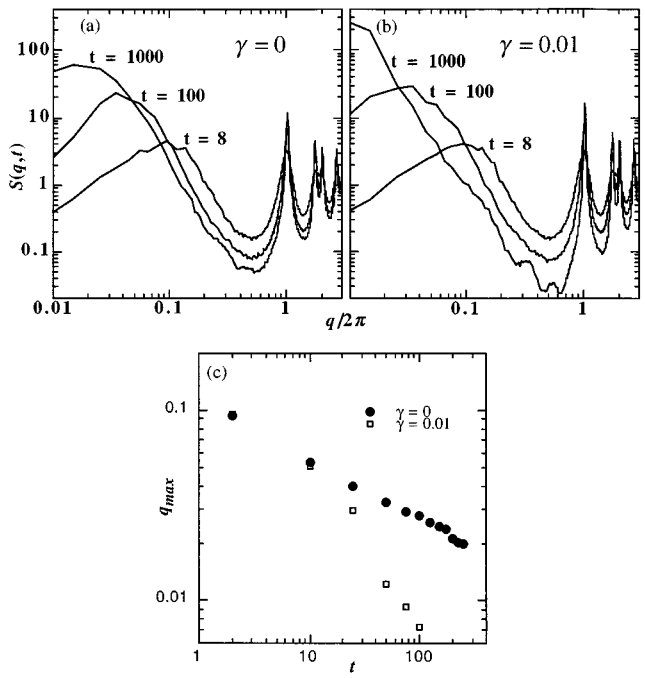

FIG. 3. Variation of $S(q)$ with time since the system was quenched to $T=0.2$, $\rho=0.325$. (a) the system at zero shear, and (b) the system subjected to a shear of $\gamma=0.01$. (c) shows the time dependence of the location of the maximum in $S(q)$. The corresponding particle configurations are shown in Fig. 2.

originates from the presence of a peak in $S(q,t)$ at low values of q—a peak indicating the existence of cluster-cluster correlations. Not much, therefore, can be learned from the actual magnitude of the slope (as is often done in dilute systems[20,23]) because the slope will depend on the shape, size, and degree of correlation *between* individual clumps of particles.[24]

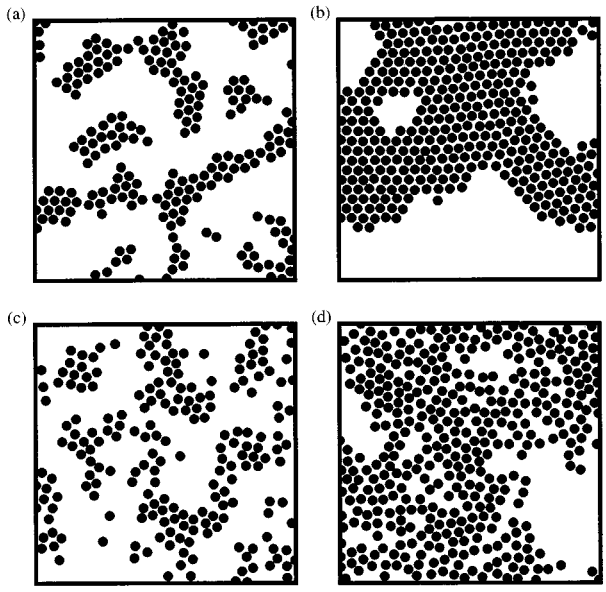

FIG. 4. Magnified view of particle configurations showing the close packed solidlike structure obtained when the system is quenched to $T=0.20$; shown are $t=8$ (a) and $t=1000$ (b). Liquidlike structures are obtained when the quench is to $T=0.45$; $t=8$ (c) and $t=1000$ (d).

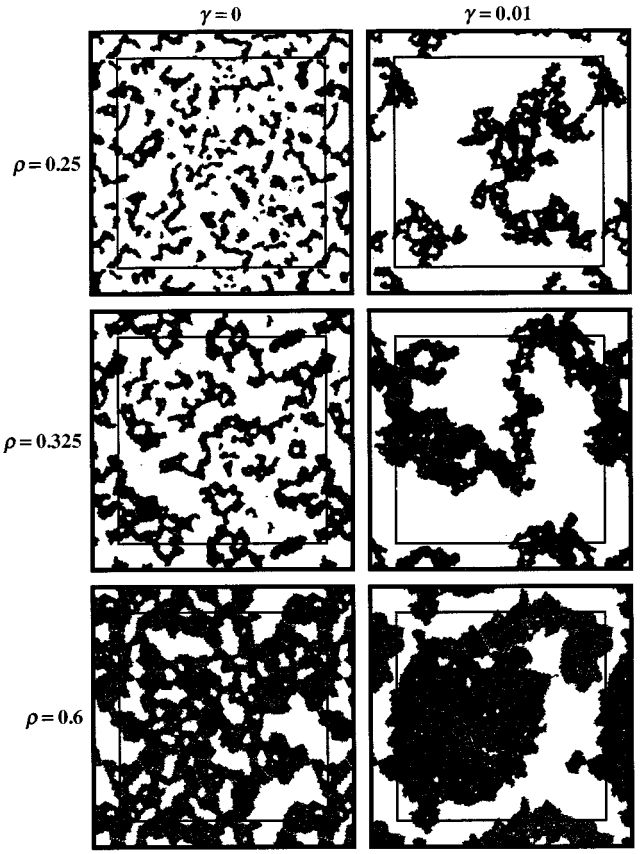

FIG. 5. Particle configurations after $t=1000$ when the system is quenched to $T=0.2$. Note that, at all three densities, the coarsening is much more rapid when a shear is applied.

The coarsening of the system is reflected by the movement of this low-q peak with time. At $t=8$, for example, $S(q,t)$ peaks at $q/2\pi\approx0.1$ which corresponds to a cluster-cluster correlation distance of about ten particle diameters. The peak increases in height and moves to a lower q as the system evolves after the quench (the signature of a coarsening process) until the system develops large clusters at $t=1000$ that nearly span the simulation box. The accelerated coarsening observed in Fig. 2 for the system at $\gamma=0.01$ could alternatively be inferred from the time variation of the location of the peak in $S(q,t)$ shown in Fig. 3(c). Here, the peak in $S(q,t)$ moves to lower q much more rapidly after the quench relative to the unsheared case.

Figure 5 displays and compares the particle configurations at the limiting time $t=1000$ for the three different post-quench densities. The influence of an applied shear on these configurations is very clear: shear greatly accelerates the coarsening. Companion plots of $S(q,t)$ from these simulations, shown in Fig. 6, confirm this observation. Figure 7, with Fig. 3, summarizes the evolution of $S(q,t)$ after quenching to the three system densities at $T=0.2$.

In 1983, Koch, Desai, and Abraham published their detailed paper on the decomposition of the LJ fluid into the vapor-liquid region of the phase diagram.[1] We repeated several of their calculations here, but for a larger system, and

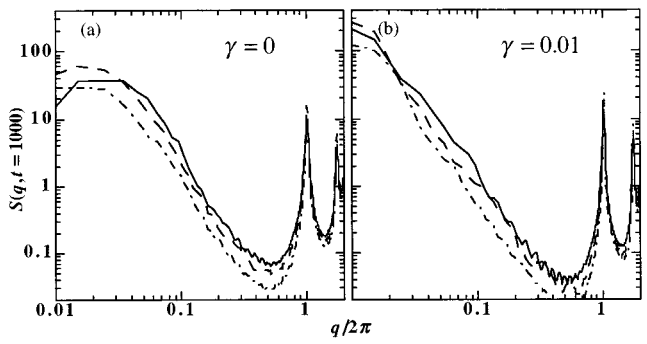

FIG. 6. Structure factors computed for each of the 6 configurations shown in Fig. 5. — $\rho=0.25$, – – – – $\rho=0.325$, – - – $\rho=0.6$.

extended that study by including a simulation of the decomposition phenomenon under shear for $\gamma=0.01$ and $\gamma=0.1$. Our data for the quench to $T=0.45$ and $\rho=0.325$ are presented in Figs. 8–11. Let us compare Fig. 8 with Fig. 2. In both cases we see the interconnected structures and we find, at even the earliest times, that the system has decomposed to two distinct phases. As time progresses, the systems coarsen. We observe temporally self-similar coarsening behavior for the system quenched to $T=0.45$ as observed at $T=0.2$. The major difference between the clusters formed after the quenches to $T=0.45$ and $T=0.2$ for $\gamma=0$ lies in the density and structure of the two phases, Fig. 4; we see that the system quenched to $T=0.45$ has clusters composed of a disordered low-density fluid whereas the quench to $T=0.2$ produces clusters of solidlike structure and density.

Figure 9 shows that the dramatic influence of the shear seen at $T=0.2$ is observed only for the higher shear rate of $\gamma=0.1$ at the quench with $T=0.45$. But that we do not see any substantial influence of the shear at the lower shear rate,

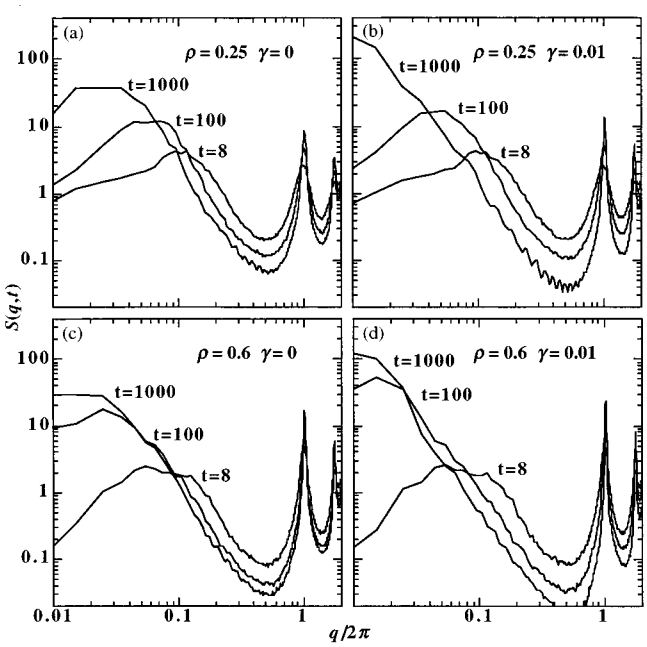

FIG. 7. Variation of $S(q)$ with time since the systems were quenched to $T=0.2$.

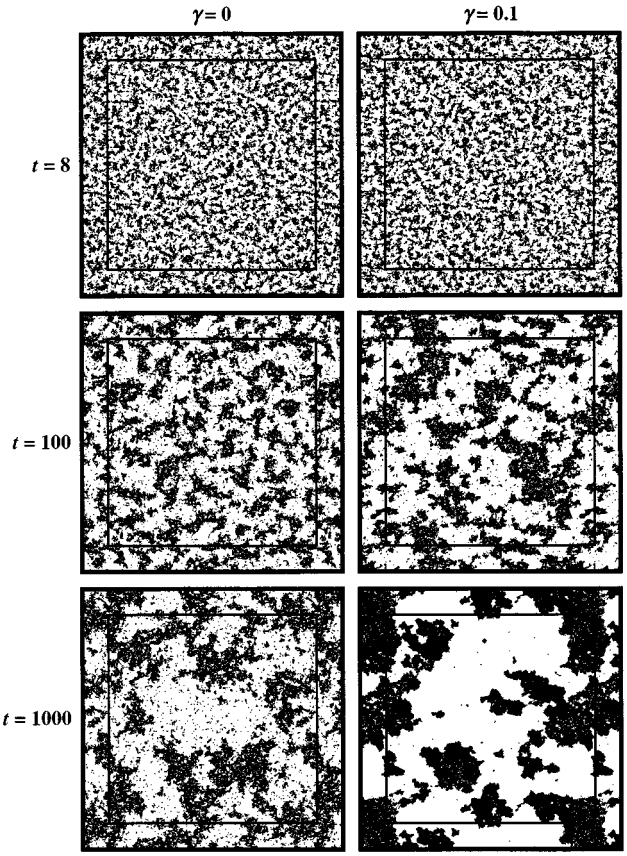

FIG. 8. Decomposition of a Lennard-Jones system of density $\rho=0.325$, quenched to a temperature $T=0.45$.

compared to results at $T=0.2$, merely reflects that the system relaxation time τ is relatively short in a system at $T=0.45$. Suppose, for convenience, we can define τ as the Maxwell relaxation time, $\tau_m=\eta/G_\infty$, with η the viscosity and G_∞ the infinite frequency shear modulus. The Maxwell relaxation time of a Lennard-Jones fluid close to freezing is $\tau_m\approx 0.2$; we estimate from calculations of the viscosity that in the liquid $\tau_m\approx 0.02$ at $T=0.45$. In general, simulations of non-Newtonian behavior in simple systems show[6] that the effects of shear are observed (i.e., the properties of the system can be shear rate dependent) when $\gamma > \tau_m^{-1}10^{-3}$. Hence it is not surprising that a shear $\gamma=0.01$ has no significant effect at the higher temperature.

The structure factors corresponding to the simulations in Figs. 8 and 9 are presented in Figs. 10 and 11. The form of $S(q,t)$ for $\gamma=0.0$ and for wave vectors $q/2\pi>1$ is that of a liquid, as one would expect from viewing the magnified real space images of Figs. 4(c) and 4(d). In Fig. 4(c) we find small clumps of liquid surrounded by a vapor and in Fig. 4(d) we find the same liquid structure but in much larger clumps. At a shear $\gamma=0.1$, however, the local structure evolves with time such that we observe a form for $S(q,t)$ characteristic of a low-density liquid at early times, but a much higher density liquid—bordering on a disordered solid phase—at $t=1000$ (Fig. 8). The long-range cluster-cluster correlations, and the growth of the clusters themselves as derived from $S(q,t)$, do not seem markedly different from that observed in the $T=0.2$ postquench simulations, as we remarked when discussing Fig. 8.

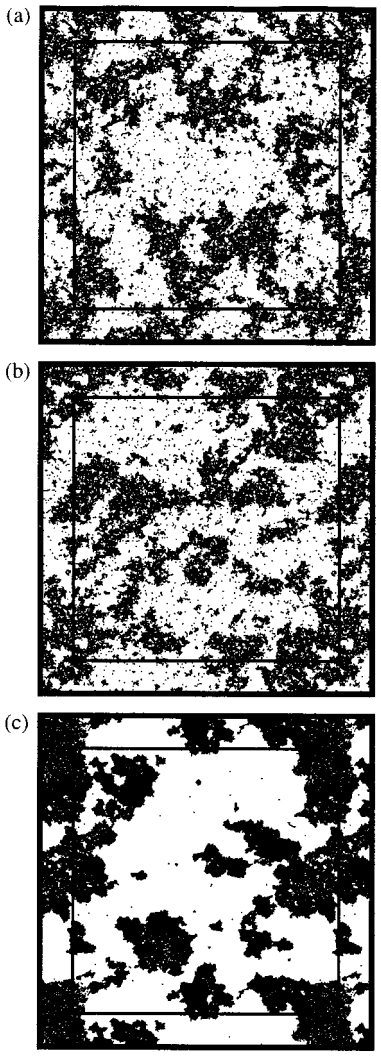

FIG. 9. Particle configurations at $t=1000$, $\rho=0.325$ for a quench to $T=0.45$. (a) no shear, (b) $\gamma=0.01$, and (c) $\gamma=0.1$. At this higher temperature only very large shear rates ($\gamma=0.1$) significantly effect the final structure.

IV. EVOLUTION OF THE STRUCTURE FACTOR: SCALING

Our comments in the previous section regarding the striking temporal self-similarity of the coarsening process in both the $T=0.20$ and $T=0.45$ quenches were based on subjective interpretations of the appearance of the particle configurations as a function of time shown in Figs. 2 and 8. The temporal self-similarity claim can, however, be cast into a more quantitative, and therefore more justified, form by deriving the expected behavior of $S(q,t)$ under such circumstances and then checking this against the simulations.[25]

If the particle configurations at different times are the same except for a change in length scale then, by definition, their structure factors will have the same form:

$$S(q,t)\sim K(q_m(t))\tilde{S}(q/q_m(t)), \tag{6}$$

where $q_m(t)$, the location of the low-q peak maximum corresponding to the cluster-cluster correlation distance, has

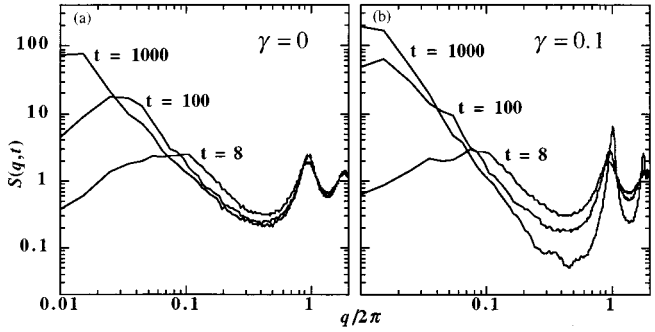

FIG. 10. Variation of $S(q,t)$ after the system was quenched to $T=0.45$, $\rho=0.325$. (a) the system at zero shear, and (b) subjected to a shear of $\gamma=0.1$.

been chosen as the characteristic scale. $\tilde{S}(x)$ is a *time-independent* characteristic structure function which has a maximum at $x=1$, and $K(q_m(t))$ is a q-independent proportionality constant. The form of $K(q_m(t))$ can be obtained by recognizing that the magnitude of the structure factor will be proportional to the number of clusters N_c present and the square of the number of scatterers per cluster n^2:

$$S(q,t)\sim N_c n^2 \tilde{S}(q/q_m(t)). \tag{7}$$

For generality we allow the clusters to be mass fractals of dimension d_f and assume that the number of scatters is proportional to the mass M of a cluster: $n\sim M\sim \xi^{d_f}\sim q_m^{-d_f}(t)$, where ξ is the cluster-cluster correlation length. Mass conservation requires $N_c n=N$, where N is the total number of particles in the system. The structure factor scaling relation is thus

$$S(q,t)\sim q_m^{-d_f}(t)\tilde{S}(q/q_m(t)). \tag{8}$$

Equation (8) is simply a more general form of the scaling relation normally given in the literature,[26,27] except that d_f has replaced the dimensionality D of the system. [Although we used the characteristic cluster-cluster correlation distance

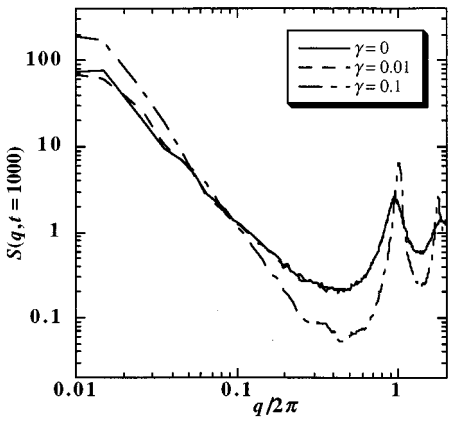

FIG. 11. Computed structure factors at $t=1000$ for the system with $\rho=0.325$ quenched to $T=0.45$. Observation of magnified portions of the particle configurations with $\gamma=0.1$ (not shown) demonstrate that the sharp peak at $q/2\pi=1$ results from nearly close packing of the disks.

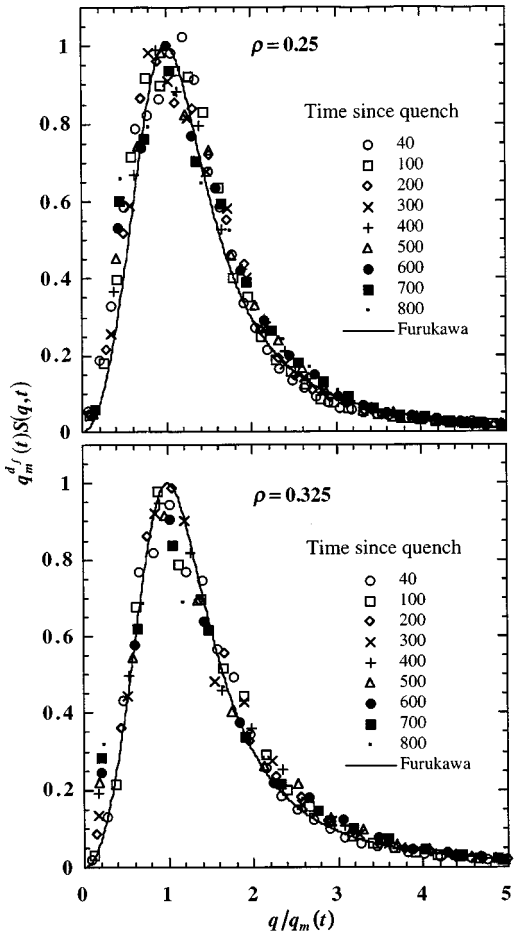

FIG. 12. Computed structure factors scaled according to Eq. (8) using $d_f = 1.85$. The quenches were to $T = 0.2$ with $\gamma = 0$ at the indicated densities. The solid line is the phenomenological theory of Furukawa (see text).

ξ and not the actual cluster size in our argument above, in a self-similar system those two quantities will be proportional, and, in fact, any measure of a characteristic distance of the system, for instance an inflection point in the structure factor peak, would be equally appropriate to use in Eq. (8).]

Figure 12 shows a plot of the structure factors for two of the systems, quenched to $T = 0.2$ as a function of time, and scaled according to Eq. (8) using, in both cases, $d_f = 1.85$. All data fall essentially on a single curve. Our description of the evolution of the system after quenching as temporally self-similar thus appears justified. The results for times earlier than $t = 40$ and later than $t = 800$ are not included in Fig. 12 because at early times the cluster growth does not completely follow a coarsening mechanism.[1] At the later times the clusters grow larger than 1/2 the simulation box size making it impossible to locate accurately the low-q peak.

The exponent used in Eq. (8) to produce Figs. 12 was not the Euclidean dimension $D = 2$. To verify that indeed $d_f \neq D$ we constructed plots of $q_m^{d_f} S(q_m)$ vs q_m for $d_f = 1.7$, 1.85, and 2 like that shown in Fig. 13. When Eq. (8) holds and d_f has been chosen properly, the points on this plot lie on a horizontal line. If d_f has not been chosen properly there will be systematic deviation away from the horizontal. It is clear that when $d_f = 2$ there is a systematic rise and when

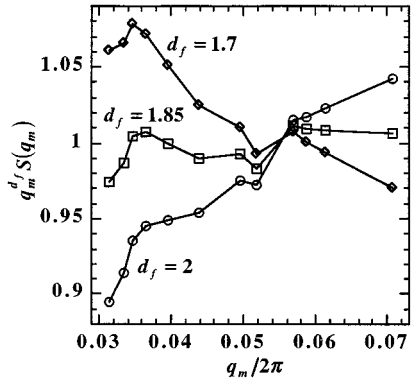

FIG. 13. The maximum in $S(q)$ for the simulation quenched to $T = 0.20$ and $\rho = 0.25$ scaled according to Eq. (8) using different values for the fractal dimension. Note that when a fractal dimension of 1.7 or 2 is assumed there is a systematic deviation from the horizontal indicating an error in the choice of d_f. In this way we obtained estimated errors for our determinations of $d_f = \pm 0.05$ in the present case.

$d_f = 1.7$ there is a systematic decrease in this plot, whereas $d_f = 1.85$ yields a nearly horizontal line. From plots such as this we estimate the accuracy in the determined fractal dimension for the systems shown in Fig. 12 to be $d_f = 1.85 \pm 0.05$.

The solid curve drawn in Fig. 12 is Furukawa's[27] phenomenological form for the characteristic structure function:

$$\tilde{S}(x) = \frac{(1+\varphi/2)x^2}{\varphi/2 + x^{2+\varphi}}. \tag{9}$$

Here we have used $\varphi = 3$ to ensure that Porod's law[28] (in two dimensions) is satisfied at high values of q. The agreement between our simulation results and this relation is impressive, especially because the only parameters used to construct Figs. 12 are the low-q peak locations at each time increment, the fractal dimension d_f, and a single, universal, normalizing constant to place the peak heights at 1. Alternatives to this characteristic function may also be considered; for example Schätzel and Ackerson's form[5] was shown to work well in colloidal systems. The particular form of the characteristic function is, however, not important for our present arguments.

Figure 14 shows the structure factor scaling for the systems quenched to $T = 0.2$, at densities $\rho = 0.25$ and $\rho = 0.325$ under the applied shear of $\gamma = 0.01$. Since the clusters grow much faster under shear, the scaling plots could only be constructed for times to about $t = 300$; beyond this it is impossible to determine accurately the low-q peak maximum given our simulation system size. Nevertheless, we find that the scaling relation still holds under shear, but that somewhat lower fractal dimensions, $d_f = 1.75 \pm 0.1$ for $\rho = 0.25$ and $d_f = 1.7 \pm 0.1$ for $\rho = 0.325$ are required to obtain a good fit. The larger error bars on these systems result from the shorter time over which we can scale the results.

Finally, scaling plots corresponding to the quenches to $T = 0.45$ are shown in Fig. 15. Here, the coarsening is slower so it is possible to scale the simulations out to $t = 1000$. Self-similar growth, however, does not appear to hold for times

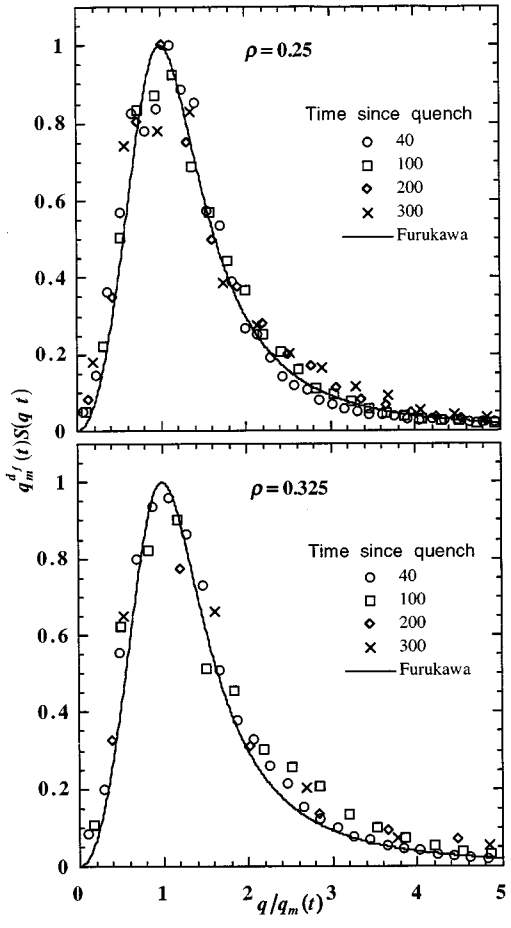

FIG. 14. Computed structure factors scaled according to Eq. (8) from simulations quenched to $T=0.2$ with an applied shear $\gamma=0.01$. Only the early times can be scaled as the cluster sizes as later times have grown too large to produce a peak in $S(q)$. $d_f=1.75\pm0.1$ and 1.7 ± 0.1 for $\rho=0.25$ and 0.325 respectively.

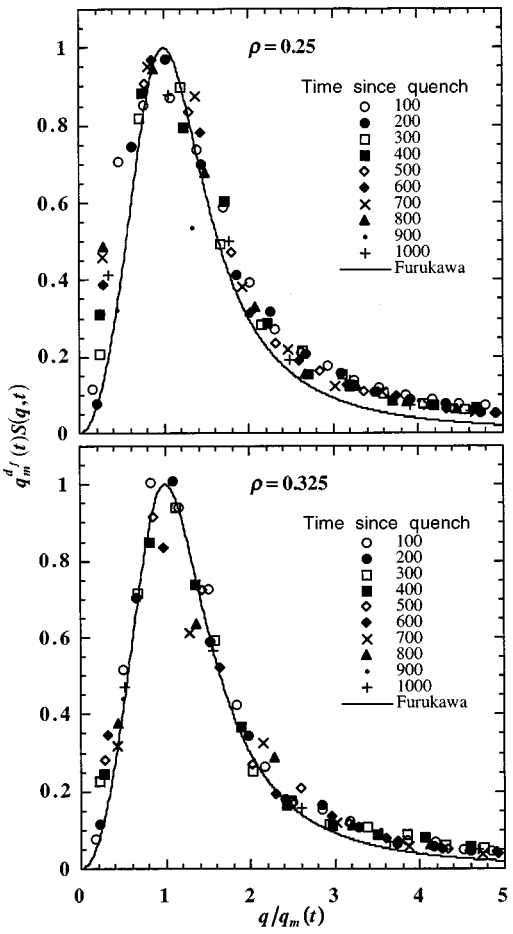

FIG. 15. Scaled $S(q)$ as in Fig. 12 except quenched to $T=0.45$. For $\rho=0.25$ $d_f=1.85\pm0.05$ and for $\rho=0.325$ $d_f=1.80\pm0.05$.

less than about $t=100$. We obtain fractal dimensions of $d_f=1.85\pm0.05$ for $\rho=0.25$ and $d_f=1.80\pm0.05$ for $\rho=0.325$. Under moderate shears of $\gamma=0.01$ the results are identical (as would be expected from the previous discussion of Fig. 9). At the higher shear rate, $\gamma=0.1$, we found that Eq. (8) does not describe the coarsening behavior over any appreciable range of times. Also, we found that at the highest density $\rho=0.6$, Eq. (8) does not describe adequately the simulation data regardless of the quench temperature or shear rate.

We repeated several of the simulations using a smaller number of particles ($N=3584$) to check the effect, if any, of system size on these results. We found that at early times the particle configurations looked similar, but that it is difficult to construct a scaling plot from Eq. (8). There are two reasons for this: (1) with the smaller system size there are fewer particles contributing to the computed $S(q)$ so it is noisier and therefore more difficult to place accurately on the scaling plot, and (2) because the systems size is smaller, $S(q,t)$ cannot be computed to the small wave vectors that can be reached with the larger system. Thus, the evolution could not be followed for long times. The result is that it is difficult to derive d_f accurately from systems much smaller than the $N=14\,336$ systems used in this study.

V. CONNECTION WITH GELS

We remarked in the Introduction that a motivation for performing the simulation work was to interpret small-angle neutron-scattering (SANS) data on the structural changes that take place as silica spheres gel.[29] The gel SANS experiments are reported in Ref. 3 so a detailed description of the experiments need not be repeated. In summary, the experimental systems were initially suspensions of silica spheres with diameter $\sigma=24$ nm, in a H_2O-D_2O medium at several volume fractions ϕ. Gelation was induced by changing the pH of the suspension and adding NaCl. SANS intensity data from the 30-m spectrometer at the NIST Cold Neutron Research Facility were obtained from the suspensions, from the final gels, and, in some cases, from the gelling system as a function of time. The suspensions and gels were also subjected to applied shears using the Couette shearing cell described in Ref. 30. The key results are reproduced graphically in Figs. 16 and 17.

Figure 16(a) plots the structure factor of the gelling $\phi=0.1$ suspension as a function of time after gel initiation at wave vectors $\leqslant q\sigma/2\pi$. At the very earliest times there is no

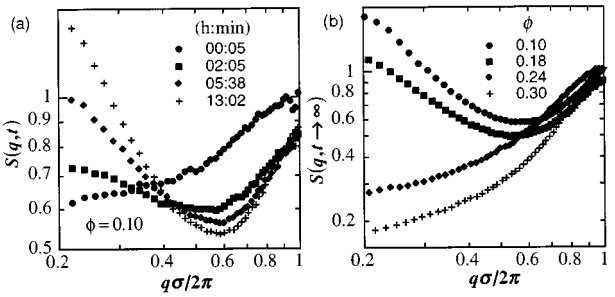

FIG. 16. Measured structure factors from SANS data on 24-nm silica spheres at $\gamma = 0$; (a) as a function of time since gel initiation at volume fraction $\phi = 0.1$ and (b) as a function of volume fraction after the gel has formed.

appreciable small-angle scattering, indicating that the initial solution is relatively homogeneous at the length scales probed by this experiment (several particle diameters). As the gelation proceeds, however, there is a marked increase in the scattering at low q, and this becomes more pronounced at longer times. At these later times, $S(q,t)$ displays a power-law increase with decreasing q (on this log-log plot the scattering increases linearly toward the origin). Compare this set of curves with the simulations of Fig. 3; the time sequences are very similar. The experiments do not detect a cluster-cluster low-q peak but, according to Fig. 3, such peaks would more likely to be observed for $q\sigma/2\pi$ less than 0.1—below the low-q limit of the present SANS experiments.

For samples with silica volume fractions above 0.18 (specifically, $\phi = 0.24$ and 0.30), the rise in the small-angle scattering, Fig. 16(b) was not observed (even in the final gels) when a shear was not applied. When shear is applied during gelation of the higher-density samples, however, this power-law increase of $S(q,t)$ returns. For example, Fig. 17 displays the structure factor for the $\phi = 0.24$ system gelled at zero shear and at a shear rate $\gamma = 4500\ \mathrm{s}^{-1}$. Furthermore, in addition to this large increase in small-angle scattering brought about by the application of shear, there is also a significant change observed in the particle-particle contact peak located near $q\phi/2\pi \approx 1$. This peak is broad and weak in the unsheared sample, but is much sharper and more intense in the sample gelled under applied shear. Compare Fig. 17 with the simulation graph of Fig. 11. The shear-influenced features in the experimental plot are replicated to a first approximation by the simulation.

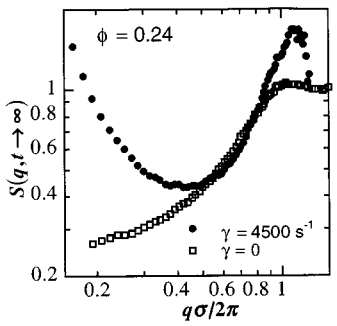

FIG. 17. Measured structure factors for a gelled sample with $\phi = 0.24$, with and without an applied shear.

VI. CONCLUSION

We have discussed the NEMD simulated decompositions of a thermostatted system, first unsheared and then subjected to planar Couette flow, after temperature quenches into the unstable vapor-liquid and the vapor-solid coexistence regions of the phase diagram. Our system was a two-dimensional system of Lennard-Jones disks, and the quenches were from the fluid to unstable state points between the critical and triple-point temperatures at $T = 0.45$, and below the triple point at $T = 0.2$.

Upon quenching, we find that a fine scale, interconnected morphology is produced at very early times in all systems, and that this initially phase-separated structure then coarsens. We can identify easily from the simulated quenches below the triple point to $T = 0.2$ a close-packed solid phase coexisting with a dilute vapor. Quenches into the region between the triple point and critical temperature display a similar morphology, but with a liquidlike phase in contact with a dense vapor. The system with a shear coarsens much more rapidly, but generally the interconnected cluster morphology is similar to that seen without shear. We did observe, however, that shear alters the structure of the dense phase after quenching to $T = 0.45$; this phase now has features of an amorphous solid.

Computations of the structure factors $S(q,t)$ as a function of time show a distinct peak at low q indicating the presence of cluster-cluster correlations, even at the earliest times after the quench. As time progresses this peak moves to smaller q and grows in height—indicating that the cluster size increases. The linear spinodal decomposition theory of Cahn-Hilliard-Cook[13] predicts a regime in which the location of the low-angle peak remains stationary while growing in amplitude. We did not observe such a regime, but this was anticipated for our system which is characterized by short-range interactions.[17]

A particularly striking feature of the observed coarsening is that, except for a change in length scale, we see that the structures at early times look similar to those at later times—that is, the cluster morphologies are temporally self-similar. Accordingly, we introduced a dynamic scaling law for $S(q,t)$, Eq. (8), generalized to allow for the presence of fractal clusters. When our simulation results are scaled by this relation, all computed structure factors fall on a single universal curve, provided that the fractal dimension d_f is chosen correctly. The scaling relation is satisfied remarkably well with $d_f = 1.85 \pm 0.05$ at both $T = 0.2$ and at $T = 0.45$ (except when $\rho = 0.325$ and $T = 0.45$ for which $d_f = 1.80 \pm 0.05$). The dynamic scaling relation also describes well the simulations quenched to $T = 0.2$ when a shear is applied, but with smaller fractal dimensions $d_f = 1.75 \pm 0.1$ for $\rho = 0.25$ and $d_f = 1.70 \pm 0.1$ for $\rho = 0.325$.

In Sec. IV we demonstrated that a thermodynamic quench into the unstable region of the phase diagram has many characteristics in common with gel initiation. For instance, gels produced from silica spheres are made by changing the pH and/or electrolyte content of a suspension so as to affect the range and nature of the particle-particle interaction potential.[20] Since a rapid change in the interaction potential is equivalent to a rapid change in the reduced temperature and density, we argued that the gelation mechanism is an

aggregation process that is similar to our quench of a system from a disordered state into an unstable two-phase region. It is particularly profitable and practical to compare the two processes because we know that cluster-cluster correlations in dense gels will dominate the scattering and make it difficult to interpret the results by conventional methods. We cannot, for example, get structural information and a fractal dimension from measurements of $S(q,t\rightarrow\infty)$ assuming that the fractal dimension is related to the rise in $S(q,t\rightarrow\infty)$ at low angles, as is done routinely for dilute gels. Equation (8), however, implies that the fractal dimension of an experimental dense system can be ascertained from the time evolution of the measured structure factor. In principle, this method will work regardless of the density of the initial suspension. To illustrate this point, we remark that Carpineti and Giglio[31] recently measured $S(q,t)$ over a very wide range of wave vectors as a function of time in dilute (volume fraction 0.03%) polystyrene colloidal solutions undergoing aggregation. They were able to determine a fractal dimension for their growing clusters in the usual way by measuring the rise in $S(q,t\rightarrow\infty)$ at intermediate wave vectors. They also measured to much lower q where they found a cluster-cluster correlation peak. A scaling plot, in the form of our Fig. 12, was constructed using the fractal dimension derived from the intermediate q measurements. All the scaled data lay on a universal curve. It is thus clear that the fractal dimension could have been derived from the scaling plot without recourse to the higher q data analysis, which required a measurement covering length scales much smaller than the cluster-cluster correlation distance yet much larger than the particle size. In short, the results of Ref. 31 and our analysis suggest that future scattering experiments on the gelation of dense colloidal systems should concentrate on measurements to wave vectors small enough to include the cluster-cluster correlation peak so that analyses based on Eq. (8) can be performed.

ACKNOWLEDGMENTS

The work was supported in part by a grant from the Office of Basic Energy Sciences, Division of Engineering and Geosciences, US Department of Energy. Butler was supported by the National Research Council. Hansen and Evans thank Fujitsu, the ANU Computer Science Department, and the ANU Supercomputer Facility for generous grants of computing time.

[1] S. W. Koch, R. C. Desai, and F. F. Abraham, Phys. Rev. A **27**, 2152 (1983).
[2] D. J. Evans and G. P. Morriss, Comput. Phys. Rep. **1**, 297 (1984); *Statistical Mechanics of Nonequilibrium Fluids* (Academic, London, 1990).
[3] C. D. Muzny, G. C. Straty, and H. J. M. Hanley, Phys. Rev. E **50**, R675 (1994).
[4] P. W. Rouw, A. T. J. M. Woutersen, B. J. Ackerson, and C. G. De Kruif, Physica A **156**, 876 (1989); R. W. Pekala and D. W. Schaefer, Macromolecules **26**, 5487 (1993).
[5] K. Schätzel and B. J. Ackerson, Phys. Rev. Lett. **68**, 337 (1992).
[6] D. J. Evans, H. J. M. Hanley, and S. Hess, Phys. Today **37** (1), 26 (1984); H. J. M. Hanley and D. J. Evans, Int. J. Thermophys. **11**, 381 (1990); *Transport Properties of Fluids: Their Correlation, Prediction, and Estimation*, edited by J. H. Dymond, J. Millat, and C. Neito de Castro (Cambridge University Press, Cambridge, England, 1995), Chap. 9, p. 249.
[7] H. J. M. Hanley and D. J. Evans, J. Chem. Phys. **76**, 3225 (1982); K. D. Romig and H. J. M. Hanley, Int. J. Thermophys. **7**, 877 (1986).
[8] M. Doi and D. Chen, J. Chem. Phys. **90**, 5271 (1989).
[9] R. Wessel and R. C. Ball, Phys. Rev. A **46**, R3008 (1992).
[10] J. A. Barker, D. Henderson, and F. F. Abraham, Physica **106**, 226 (1981).
[11] A. Z. Panagiotopoulos, Int. J. Thermophys. **6**, 1057 (1994).
[12] D. Henderson, Mol. Phys. **34**, 301 (1977).
[13] J. W. Cahn and J. E. Hilliard, J. Chem. Phys. **28**, 258 (1958); **31**, 688 (1959); Acta Metall. **19**, 151 (1971); J. W. Cahn, J. Chem. Phys. **30**, 1121 (1959); H. E. Cook, Acta Metall. **18**, 297 (1970).
[14] J. W. Cahn, J. Chem. Phys. **42**, 93 (1964).
[15] J. S. Langer, M. Bar-On, and H. D. Miller, Phys. Rev. A **11**, 1417 (1975).
[16] F. Abraham, J. Chem. Phys. **63**, 157 (1975).
[17] K. Binder, Phys. Rev. A **29**, 341 (1984).
[18] M. Grant, M. San Miguel, J. Vinals, and J. D. Gunton, Phys. Rev. B **31**, 3027 (1985); J. D. Gunton, M. San Miguel, and P. S. Sahni, in *Phase Transitions and Critical Phenomena*, edited by C. Domb and J. L. Lebowitz (Academic, London, 1983), Vol. 8.
[19] B. D. Gaulin, S. Spooner, and Y. Morii, Phys. Rev. Lett. **59**, 668 (1987).
[20] See, for example, C. J. Brinker and G. W. Scherer, *Sol-Gel Science: The Physics and Chemistry of Sol-Gel Processing* (Academic, San Diego, 1990).
[21] D. C. Rapaport, Comput. Phys. Rep. **9**, 1 (1988).
[22] B. D. Butler and T. R. Welberry, J. Appl. Crystallogr. **25**, 391 (1992).
[23] D. W. Schaefer, J. E. Martin, P. Wiltzius, and D. S. Cannell, Phys. Rev. Lett. **52**, 2371 (1984); G. Dietler, C. Aubert, D. S. Cannell, and P. Wiltzius, *ibid*. **57**, 3117 (1986).
[24] B. D. Butler, H. J. M. Hanley, C. D. Muzny, and G. C. Straty, in *Neutron Scattering in Materials Science II*, edited by Dan A. Neumann, Thomas P. Russell, and Bernhard J. Wuensch, MRS Symposia Proceedings No. 376 (Materials Research Society, Pittsburgh, 1996), p. 323.
[25] B. D. Butler, H. J. M. Hanley, D. Hansen, and D. J. Evans, Phys. Rev. Lett. **74**, 4468 (1995).
[26] K. Binder and D. Stauffer, Phys. Rev. Lett. **33**, 1006 (1974); J. Marro, J. L. Lebowitz, and M. H. Kalos, *ibid*. **43**, 282 (1979); J. D. Gunton, M. San Miguel, and P. S. Sahni, *Phase Transitions and Critical Phenomena* (Academic, London, 1983), Vol. 8, p. 267; G. S. Grest and D. J. Srolovitz, Phys. Rev. B **30**, 5150 (1984).
[27] H. Furukawa, Adv. Phys. **34**, 703 (1985).
[28] G. Porod, *Small Angle X-ray Scattering*, edited by O. Glatter and O. Kratky (Academic, London, 1982), Chap. 2.
[29] C. D. Muzny, D. Hansen, G. C. Straty, D. J. Evans, and H. J. M. Hanley, Int. J. Thermophys. **16**, 337 (1995).
[30] G. C. Straty, H. J. M. Hanley, and C. J. Glinka, J. Stat. Phys. **62**, 1015 (1991).
[31] M. Carpineti and M. Giglio, Phys. Rev. Lett. **68**, 3327 (1992).